Prewetting and density fluctuations in the prewetting supercritical phase

1998 J. Phys.: Condens. Matter 10 9431

(http://iopscience.iop.org/0953-8984/10/42/009)

J. Phys.: Condens. Matter **10** (1998) 9431–9442. Printed in the UK PII: S0953-8984(98)92163-4

Prewetting and density fluctuations in the prewetting supercritical phase

K Omata† and F Yonezawa

Department of Physics, Faculty of Science and Technology, Keio University, 3-14-1 Hiyoshi Kohoku-ku, Yokohama 223-8852, Japan

Received 27 February 1998, in final form 13 July 1998

Abstract. By means of Monte Carlo simulations, we investigate prewetting and its supercritical phase. First, we examine several fluid–substrate interaction parameters, and discuss the general properties of prewetting. We locate a prewetting line for each parameter and obtain global phase diagrams. Secondly, we study the prewetting supercritical phase, in which density fluctuations in a film play an important role. From the structure factors of the first adsorption layer, we derive isotherms of two-dimensional compressibility and the extension of the prewetting line defined by mapping out the locus of points at which the compressibility attains its maximum value. It is shown that the prewetting line and its extension bend one another at the prewetting critical point. Our results lend support to recent mercury-on-sapphire experiments.

1. Introduction

There have been quite a number of studies on wetting transitions [1–3], since theoretical predictions were made in 1977 by Cahn [4], and Ebner and Saam [5]. However, it is only since 1992 that prewetting has been detected experimentally by quartz microbalances in helium-on-caesium [6] and hydrogen-on-rubidium systems [7], by ellipsometry in a cyclohexane–methanol mixture [8], by optical reflectivity measurements in a mercury-on-sapphire system [9–12], and by means of velocity of sound measurements in mercury-on-molybdenum and mercury-on-niobium systems [13]. In these experiments, the thickness of the wetting film or the amount of adsorbates has been estimated.

Let us consider a fluid system in the gas phase, and increase the pressure at constant temperature. When there is a substrate which interacts with fluid particles attractively, a film is formed on the substrate, and its thickness increases with pressure. If the thickness changes discontinuously at a certain pressure *in the gas phase*, this behaviour is called prewetting. The system undergoes a thin-to-thick-film transition. Prewetting is observed in a certain temperature range, and a prewetting line (PWL) is determined from sets of such temperatures and pressures (figure 1(a)). One edge of the PWL is located on the gas–liquid coexistence curve, and the wetting temperature T_w is defined at this location.

The other edge of the PWL is the prewetting critical point (CPW). Beyond the prewetting critical temperature T_{cpw}, there is no longer any discontinuous change. This region is the prewetting supercritical phase (figure 1(b)), in which density fluctuations must be taken

† Present address: Faculty of Science and Technology, Keio University, Shin-Kawasaki Mitsui Building W.3F, 890-12 Kashimada, Saiwai-ku, Kawasaki 211-0958, Japan. Telephone: +81-44-520-6033; fax: +81-44-541-5919; e-mail: omata@rk.phys.keio.ac.jp.

0953-8984/98/429431+12$19.50

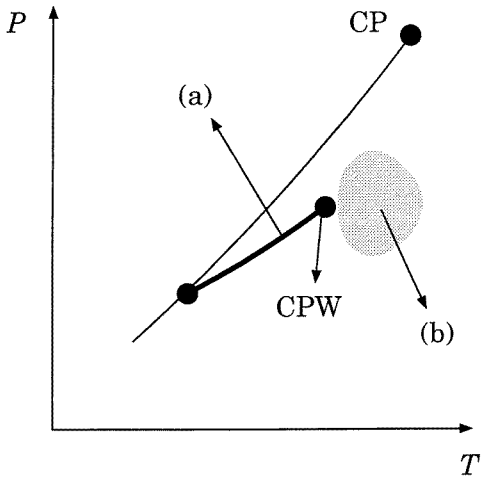

Figure 1. The schematic P–T phase diagram; (a) the prewetting line, and (b) the prewetting supercritical region.

into account. In the vicinity of the CPW, relatively large droplets are expected to form on the substrate, and the wetting behaviours in this region should be called two-dimensional critical phenomena. Experimentally, the prewetting supercritical phase has been identified by Rutledge and Taborek in a helium-on-caesium system [6], and, recently, Yao and Hensel have also studied this phase in a mercury-on-sapphire system [12]. However, apart from these experimental studies, this phase has attracted little attention so far.

This article deals with prewetting, and seeks to address some problems of its supercritical phase. For that purpose, we carry out Monte Carlo (MC) simulations, the model and method for performing which are described in section 2. In section 3, we discuss the general properties of prewetting. A detailed investigation becomes possible from the study of a large number of thermodynamic and interaction parameters. On the basis of an examination of prewetting, the prewetting supercritical region is then studied, in section 4. The use of a relatively large-size system allows us to perform a microscopic analysis of two-dimensional (2D) structures in a film. To what extent our simulations can explain behaviours in this phase is our main interest. The final section is devoted to a summary.

2. The model and method

We carry out off-lattice isobaric–isothermal MC simulations of a Lennard-Jones system. This method has been developed by Finn and Monson, and shown to be effective in the study of inhomogeneous systems such as a system undergoing a wetting transition [14, 15]. In this work, several improvements are introduced:

(i) the use of a relatively large system size, i.e., the number of particles $N = 12\,500$ and the simulation-box size $50\sigma \times 50\sigma \times L_z$, where σ is defined in equation (1) and L_z is varied via the MC sequence (3) described below;

(ii) the long computation time, 2×10^3–8×10^4 MC steps; and

(iii) examination of lots of interaction and thermodynamic parameters.

These allow us to perform a detailed and microscopic data analysis.

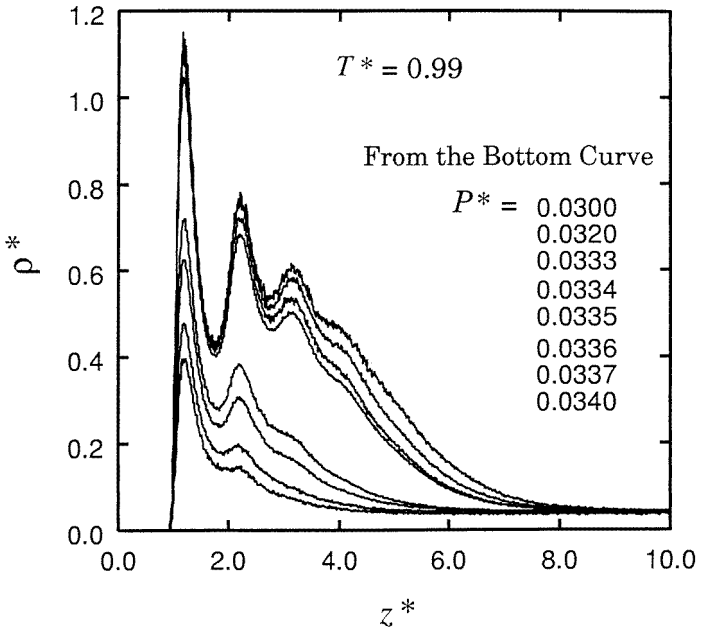

Figure 2. Density profiles for $\varepsilon_w^* = 2.0$ and $T^* = 0.99$.

As the interparticle interaction, we choose a familiar Lennard-Jones (LJ) 12–6 potential with the cut-off distance 2.5σ:

$$\phi_p(r_{ij}) = \begin{cases} 4\varepsilon\left[\left(\dfrac{\sigma}{r_{ij}}\right)^{12} - \left(\dfrac{\sigma}{r_{ij}}\right)^{6}\right] & r_{ij} \leqslant 2.5\sigma \\ 0 & r_{ij} > 2.5\sigma. \end{cases} \tag{1}$$

The particle–substrate interaction is also chosen to be in a LJ form; considering a flat substrate, we apply the following form obtained from an appropriate integration of the LJ 12–6 potential:

$$\phi_w(z_i) = \frac{3\sqrt{3}\,\varepsilon_w}{2}\left[\left(\frac{\sigma_w}{z_i}\right)^{9} - \left(\frac{\sigma_w}{z_i}\right)^{3}\right] \tag{2}$$

where z_i denotes the distance from the solid surface to the ith particle. A periodic boundary condition is applied in the x–y direction, and we locate an attractive surface at $z = 0$ which interacts with a particle through equation (2), and a repulsive ceiling at $z = L_z$. In the off-lattice isobaric–isothermal MC method due to Finn and Monson, one MC step consists of three sequences:

(1) N attempted random particle translations;
(2) N attempted small particle translations; and
(3) one attempted volume displacement.

Note that, in the procedure (1), we select a particle and randomly change its coordinates by amounts which are limited only by the size of the simulation cell and not by a fixed maximum displacement. In the procedure (2), we select a particle and attempt to translate it by a distance $\Delta r/\sigma$ less than 0.5. In order to study isothermal behaviours, we carry out

a series of runs with increasing pressure $P^* \equiv \sigma^3 P/\varepsilon$ at constant temperature $T^* \equiv kT/\varepsilon$. Hereafter, an asterisk is added to a variable normalized with respect to σ and ε.

3. Prewetting

First, we investigate the behaviours of prewetting in this section.

We show typical density profiles $\rho^*(z^*)$ for $\varepsilon_w^* = 2.0$ in figure 2, where the pressure is increased in the gas phase at constant temperature $T^* = 0.99$. The observed oscillation is due to a packing effect, and the number of adsorption layers can be roughly obtained by counting the number of the peaks. In the low-pressure range $P^* \leqslant 0.0334$, we can see a small first peak followed by a tail, indicating that the first adsorption layer is filled incompletely, and that the substrate is partially wet. Although the density profile grows gradually with pressure, it remains small in this pressure range. At $P^* = 0.0335$, $\rho^*(z^*)$ is transformed discontinuously. The first adsorption layer is filled up, and a jump is found in the number of layers and the amount of adsorbates. This behaviour is thought to be prewetting, because the change is discontinuous despite the fact that we make the pressure increment smaller around this pressure. The density profile grows gradually again beyond this pressure, until the system reaches the gas–liquid coexistence state.

From figure 2, we calculate the adsorption excess density, defined as

$$\Gamma^* \equiv \int_0^{L_z^*} \mathrm{d}z^* \, [\rho^*(z^*) - \rho_b^*] \tag{3}$$

where ρ_b^* is the bulk density; we estimate this by evaluating the gas density far from our substrates at $z^* = 0$ and $z^* = L_z^*$. We show curves of P^* versus Γ^* in figure 3—that is,

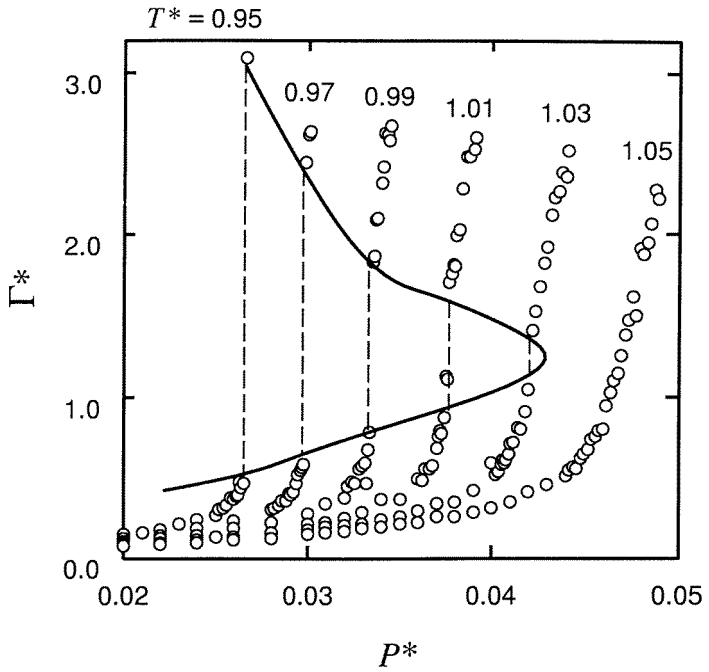

Figure 3. Adsorption isotherms for $\varepsilon_w^* = 2.0$.

adsorption isotherms. It is found that the adsorption isotherms for the temperature range $0.95 \leqslant T^* \leqslant 1.03$ change discontinuously along the broken lines, which implies that prewetting takes place. The magnitude of the jump gets smaller with temperature, and the change is continuous for $T^* > 1.03$. From this observation, we can determine the wetting temperature: $T_w^* \simeq 0.95$, and the prewetting critical temperature: $T_{cpw}^* \simeq 1.03$. The solid curve is the boundary of two two-phase regions, i.e., the region of thin-film and liquid phases for $P^* < 0.0264$, and that of thin-film and thick-film phases for $0.0264 < P^* < 0.0422$, where $P^* = 0.0264$ is the saturation pressure corresponding to T_w^*. A film is unstable inside the curve.

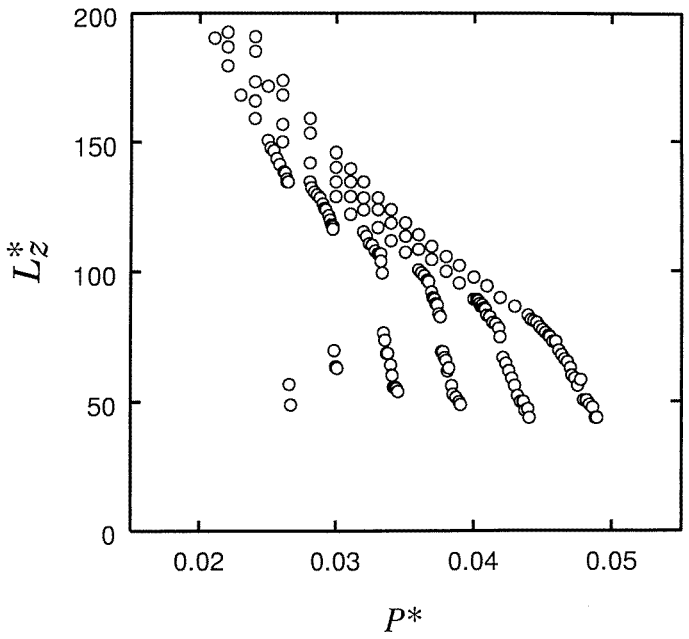

Figure 4. The mean value of L_z^* for $\varepsilon_w^* = 2.0$. Starting from the left-hand side, $T^* = 0.95$, 0.97, 0.99, 1.01, 1.03, and 1.05.

In order to see how L_z^* is varied via MC procedure (3) described in section 2, we present its mean value in figure 4. It is found that L_z^* decreases with pressure, and shows a jump when prewetting occurs.

The results are summarized in the phase diagrams of figure 5. Figure 5(a) is the phase diagram in P^*–$1/\Gamma^*$–ε_w^* space, where the results for several values of ε_w^* are included. The thick solid curves are the boundaries of the two two-phase regions, as in figure 3, and form the boundary surface shaded with dots. In this figure, the right-hand and left-hand regions of the solid curves are the thin-film and thick-film phases, respectively. We find that the thick-film phase is reduced as ε_w^* is decreased, and we can no longer observe prewetting for $\varepsilon_w^* < 1.8$, but observe critical wetting. This is because the interparticle interaction is made short range by the cut-off radius (equation (1)) [16].

Figure 5(b) shows the $\Delta\mu^*$–T^* surface of the phase diagram, where $\Delta\mu^* \equiv kT^* \ln(P^*/P_0^*)$ is the chemical-potential difference of an ideal gas from its value at gas–liquid coexistence and P_0^* is a saturation pressure calculated from the modified Benedict–Webb–Rubin (MBWR) equation of state for a LJ system with the cut-off length 2.5σ

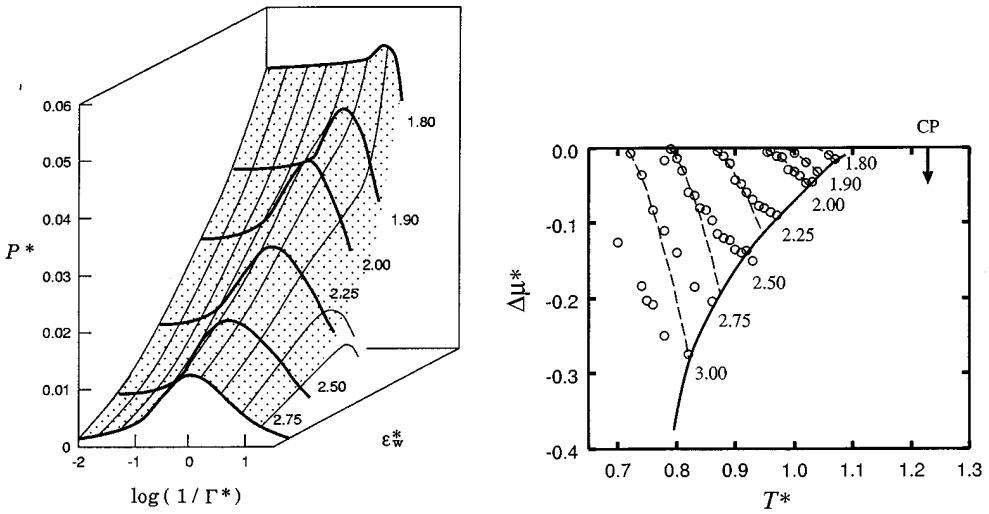

Figure 5. The phase diagram in (a) P^*–$1/\Gamma^*$–ε_w^* and (b) $\Delta\mu^*$–T^* space. The bulk critical point is denoted by CP.

[15, 17]. The PWL is moved toward the bulk triple point as ε_w^* increases, because a thick film is easily formed. For $\varepsilon_w^* \geqslant 3.0$, T_w^* seems to be lower than the triple-point temperature $T_t^* \simeq 0.68$. On the other hand, the PWL is moved toward the bulk critical point as ε_w^* is decreased, and, at the same time, it shrinks with decrease in its length and slope. This shrinkage corresponds to the reduction of the thick-film phase in figure 5(a). The solid line connects the CPWs for each ε_w^*, and the broken lines show the scaling relation of a PWL, $-\Delta\mu^* \sim (T^* - T_w^*)^{3/2}$ [18]. Although simulations of high accuracies are required to discuss agreements with this relation, we can see that each plot tends to fit closely with the scaling relation in the vicinity of the wetting temperature, and to deviate from it for large $|\Delta\mu^*|$ around the CPW.

4. The prewetting supercritical phase

Since the 1980s, Hensel and Yao have found for a mercury-on-sapphire system that the optical reflectivity from the sapphire window exhibits an anomalous increase in the gas phase near the bulk critical point [19–21]. This behaviour has been attributed to the formation of dense mercury clusters, and the line on which the reflectivity starts to increase has been called the 'Marburg line' [21–24]. An interesting point is that this line bends, and there are two temperature ranges. For the low-temperature range, they have reinterpreted the reflectivity anomaly as a consequence of prewetting. They have estimated the thickness of a film from the reflectivity data, and a prewetting line has been determined [9–12]. On the other hand, for the high-temperature range, they assume that this line corresponds to the maximum in the 2D compressibility of the prewetting supercritical one-phase region [12], which is based on the results of helium-on-caesium experiments [6]. This is exactly what we prove by means of a microscopic analysis of the simulation data in this section.

As shown in the last section, the adsorption isotherms increase continuously in the prewetting supercritical region. For a more detailed analysis, we divide the film into

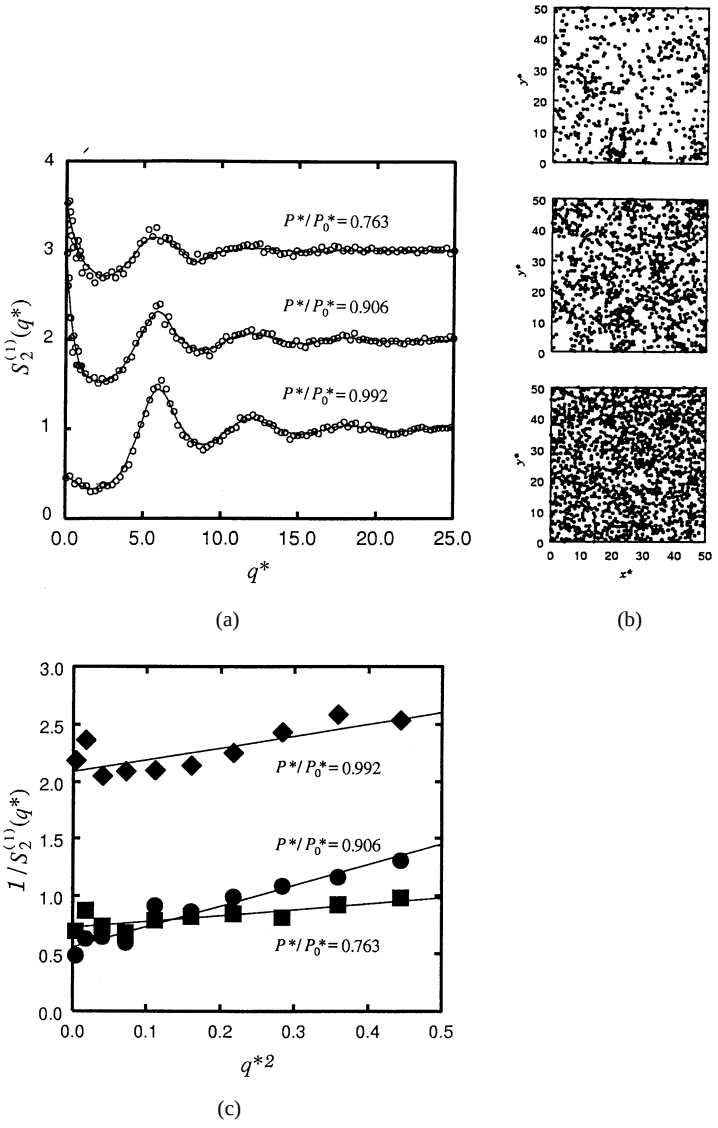

Figure 6. (a) The structure factor of a first adsorption layer for $\varepsilon_w^* = 2.0$ and $T^* = 1.06$; the curves are shifted for clarity by 2 and by 1 for the lowest and intermediate pressure, respectively, (b) a 'snapshot' for each state, and (c) the Ornstein–Zernike–Debye plot.

adsorption layers and observe the 2D structures in them. In order to see whether the substrate is wet or not, it is important to investigate the structure of the first adsorption layer. To this end, we calculate a 2D structure factor of the first layer:

$$S_2^{(1)}(q^*) \equiv \left\langle \frac{1}{N^{(1)}} \left[\left(\sum_i \cos \boldsymbol{q}^* \cdot \boldsymbol{R}_i^* \right)^2 + \left(\sum_i \sin \boldsymbol{q}^* \cdot \boldsymbol{R}_i^* \right)^2 \right] \right\rangle \tag{4}$$

$$\boldsymbol{q}^* \equiv \frac{2\pi}{L^*}(\nu_1, \nu_2) \qquad \nu_1, \nu_2\text{: integer} \tag{5}$$

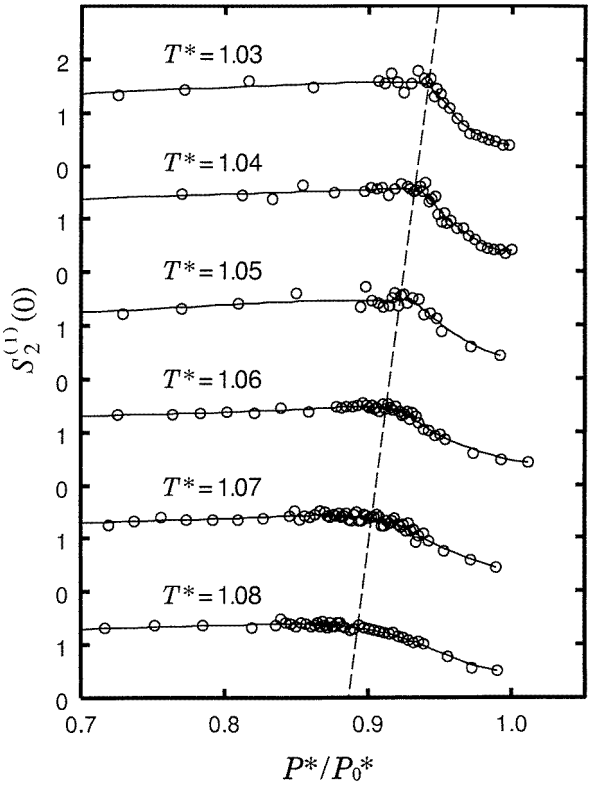

Figure 7. Isotherms of $S_2^{(1)}(0)$ for $\varepsilon_w^* = 2.0$.

where $N^{(1)}$ is the number of particles in the first layer, $L^* = L_x/\sigma = L_y/\sigma = 50$, and $\boldsymbol{R}_i^* \equiv (x_i^* \equiv x_i/\sigma, y_i^* \equiv y_i/\sigma)$ is the x–y coordinate of the ith particle.

In figure 6(a), we show typical structure factors for different pressures at $T^* = 1.06 > T_{cpw}^*$. When the pressure is low ($P^*/P_0^* = 0.763$), $S_2^{(1)}$ oscillates around 1.0, implying that adsorbed particles form a 2D gas state of small droplets. The situation is demonstrated by the top panel of figure 6(b), in which the 'snapshot' of the first adsorption layer is depicted. When the pressure is in the intermediate range ($P^*/P_0^* = 0.906$), the oscillation is enhanced, and some characteristic features appear:

(1) a relatively sharp rise for small q^*, which indicates a build-up of long-range order such as a formation of large droplets (see the middle panel of figure 6(b)); and

(2) the oscillation for large q^*, which reflects short-range order in droplets.

When the pressure is high ($P^*/P_0^* = 0.992$), $S_2^{(1)}$ shows liquid-like properties specified by the oscillation at large q^*. The film is thick, and the density of the first layer is large (see the bottom panel of figure 6(b)).

Here, the small-q^* behaviour at intermediate pressure is noteworthy. A simple way to analyse this behaviour is to fit the data approximately with the Ornstein–Zernike relation:

$$S_2^{(1)}(q^*) = \frac{S_2^{(1)}(0)}{1 + \xi_{\parallel}^{*2} q^{*2}} \tag{6}$$

even though a number of approximations have been proposed for the 2D Ising system [25].

In fact, the system is three dimensional, and, strictly speaking, it is a 'quasi-2D' feature that we intend to derive. In figure 6(c), the so-called Ornstein–Zernike–Debye plot is given, where $1/S_2^{(1)}$ is shown as a function of q^{*2}. By means of a least-mean-squares fitting and extrapolation, we determine $S_2^{(1)}(0)$, and find that this value is at its largest at intermediate pressure, as can also be seen from figure 6(a).

By performing the same analysis for various pressures and temperatures, we obtain isotherms of $S_2^{(1)}(0)$ for $1.03 \leqslant T^* \leqslant 1.08$ as shown in figure 7. We can see that each isotherm reaches its maximum point at a certain pressure. Let us address the behaviour in figure 7 described as a 2D critical phenomenon, because it takes place in the region slightly above the CPW. As for the bulk critical phenomena, $S_2^{(1)}(0)$ describes the compressibility, and increases near the CPW. The physical picture given by the above result is that, when the pressure is increased, the size of the droplets is increased, and the dry region of the substrate or the distance among droplets is decreased. This causes the substrate to start to be wet at a pressure at which $S_2^{(1)}(0)$ reaches its maximum. The high-pressure range from this pressure to the saturation pressure is the region in which the substrate is covered by a wetting film, and the density of the first adsorption layer is large. Accordingly, the 2D compressibility of the first layer is small in this region, which leads to the decrease of $S_2^{(1)}(0)$. In the case of mercury-on-sapphire experiments, one expects the filling up of the first adsorption layer to cause the optical reflectivity to start to increase. From these considerations, we can suggest that the pressure range near the saturation pressure, at which the reflectivity increases, corresponds to the pressure region in which $S_2^{(1)}(0)$ decreases.

The broken line in figure 7 connects the maximum points of the isotherms, which are found to shift toward small P^*/P_0^* with temperature. By mapping out the locus of these points, we can define an extension of the PWL. This extension is shown as the squares plot in the phase diagram given as figure 8 for $\varepsilon_w^* = 2.0$. We can see that the PWL and its extension bend each other at the CPW, and this feature is in qualitatively good agreement with the mercury-on-sapphire result. The same phase diagram feature is obtained for other values of ε_w^*.

Note that the 2D compressibility can be also estimated from the fluctuation of the excess surface density:

$$\chi \equiv \frac{1}{T^*} \frac{\langle \Gamma^{*2} \rangle - \langle \Gamma^* \rangle^2}{\langle \Gamma^* \rangle}. \tag{7}$$

We display isotherms of χ in figure 9, and we find that the result in figure 7 is more satisfactory, even though the pressures which provide the maximum of $S_2^{(1)}(0)$ and χ are nearly consistent. In order to estimate the compressibility from equation (7), we require a larger system size and a lot of simulation time. This is another reason for dividing a film and studying its 2D structure.

5. Summary

In this work, we have studied prewetting and its supercritical phase by means of an isobaric–isothermal MC method.

The main result in the first part of this article is the phase diagrams illustrated in figure 5. To date, such phase diagrams have only been proposed theoretically [26–28], while we have reproduced the equivalent result via computer simulations in this work, and discussed general properties of prewetting. We have been able to do this by means of examination of the large number of interaction and thermodynamic parameters.

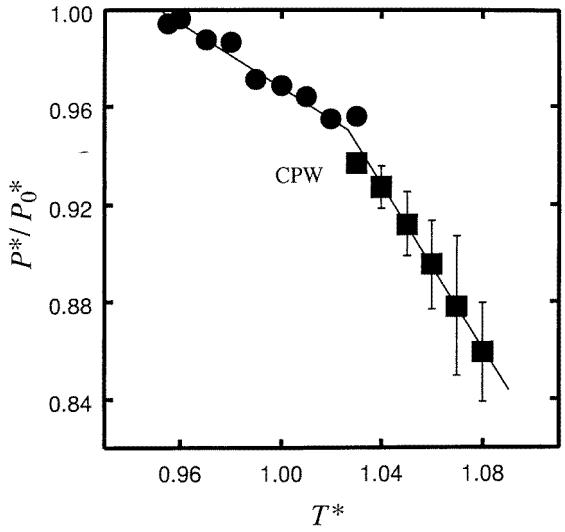

Figure 8. The phase diagram on the P^*/P_0^*–T^* surface for $\varepsilon_w^* = 2.0$, including the prewetting supercritical region. The circles plot is the PWL provided in section 3.

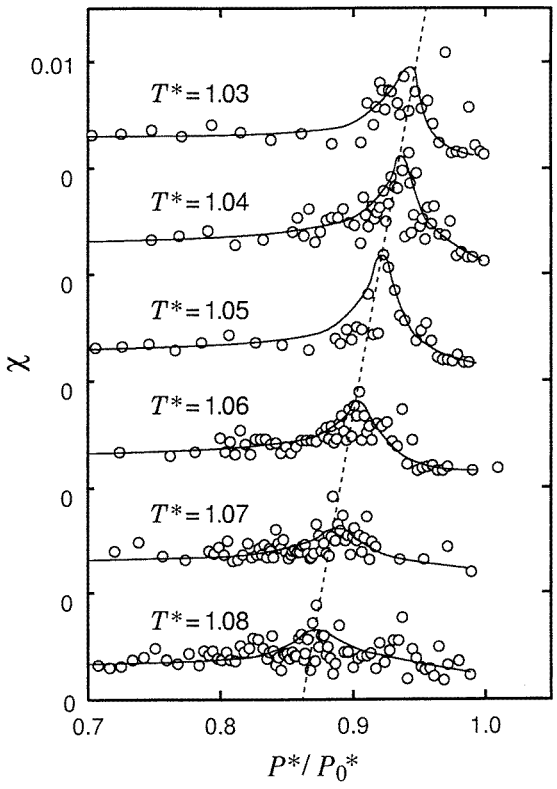

Figure 9. Isotherms of χ for $\varepsilon_w^* = 2.0$.

The study in the first part was also the starting point for the analysis in the second part of this article, where we dealt with the prewetting supercritical phase. Through the use of a relatively large-size system, we performed a microscopic analysis of 2D structures in a film, and confirmed that the extension of the prewetting line marks the maximum of the compressibility in this region.

From these results, we can understand that the anomaly of the optical reflectivity in mercury-on-sapphire experiments arises from wetting by mercury of the sapphire window in both the low- and high-temperature ranges of the Marburg line. Furthermore, we can suggest that the property of the phase diagram of the bending at the CPW is regarded as a feature of wetting phenomena. It is true that the LJ interactions are not realistic for a mercury-on-sapphire system. However, our assertion as regards this point is that the behaviour observed in a mercury-on-sapphire system is a general property, which is somehow independent of the details of the interaction forms. In fact, Rutledge and Taborek found a similar behaviour in a helium-on-caesium system [6]. Another point that we would like to make is that even the LJ interactions give the essential aspects of the wetting phenomena. The results obtained in this work suggest that, for our purposes, the LJ interactions are appropriate, at least as a first approximation.

Finally, we mention a few controversial subjects.

(1) In a mercury-on-sapphire system, the CPW is located in the vicinity of the bulk critical point ($T_{cpw} = 1741$ K and $T_c = 1751$ K). Therefore, it is possible that the bulk critical phenomena have an influence on the behaviours in the prewetting supercritical phase.

(2) Hensel and Yao have suggested that there is a close relation between the prewetting line in the gas phase and the metal–nonmetal transition line in the liquid phase, and interpreted this as indicating that prewetting results from the change of the interatomic interaction, followed by the change of the electronic structure of mercury [9–12].

(3) The origin of the bending property is not yet clear.

Acknowledgments

Computer resources were kindly made available by the ‘Research for the Future’ Project at Keio University (JSPS-RFTF96I00102). We would like to thank M Yao, F Hensel, K Tsuji, and S Dietrich for helpful discussions.

References

[1] Sullivan D E and Telo da Gama M M 1986 *Fluid Interfacial Phenomena* ed C A Croxton (New York: Wiley) p 45
[2] Dietrich S 1988 *Phase Transitions and Critical Phenomena* vol 12, ed C Domb and J Lebowitz (London: Academic) p 1
[3] Schick M 1990 *Liquids at Interfaces (Les Houches Session XLVIII)* ed J Charvolin, J F Joanny and J Zinn-Justin (Amsterdam: North-Holland)
[4] Cahn J W 1977 *J. Chem. Phys.* **86** 3667
[5] Ebner C and Saam W F 1977 *Phys. Rev. Lett.* **38** 1486
[6] Rutledge J E and Taborek P 1992 *Phys. Rev. Lett.* **69** 937
[7] Mistura G, Lee H C and Chan H M W 1994 *J. Low. Temp. Phys.* **96** 221
[8] Kellay H, Bonn D and Meunier J 1993 *Phys. Rev. Lett.* **71** 2607
[9] Hensel F and Yao M 1994 *Elementary Processes in Dense Plasmas* ed S Ichimaru and S Ogata (Tokyo: Addison-Wesley)
[10] Hensel F 1995 *Adv. Phys.* **44** 3
[11] Hensel F and Yao M 1996 *J. Non-Cryst. Solids* **205–207** 231
[12] Yao M and Hensel F 1996 *J. Phys.: Condens. Matter* **8** 9547

[13] Kozhevnikov V F, Arnold D I, Naurzakov S P and Fisher M E 1997 *Phys. Rev. Lett.* **78** 1735
[14] Finn J E and Monson P A 1988 *Mol. Phys.* **65** 1345
[15] Finn J E and Monson P A 1989 *Phys. Rev.* A **39** 6402
[16] Dietrich S 1998 private communication
[17] Nicolas J J, Gubbins K E, Street W B and Tildesley D J 1979 *Mol. Phys.* **37** 1429
[18] Nightingale M P, Saam W F and Schick M 1984 *Phys. Rev.* B **30** 3830
[19] Hefner W and Hensel F 1982 *Phys. Rev. Lett.* **48** 1026
[20] Hefner W, Sonneborn-Schmick B and Hensel F 1982 *Ber. Bungenges. Phys. Chem.* **86** 844
[21] Yao M, Uchtmann H and Hensel F 1985 *Surf. Sci.* **465** 156
[22] Hernandez J P 1982 *Phys. Rev. Lett.* **48** 1682
[23] Turkevich L A and Cohen M H 1984 *J. Phys. Chem.* **88** 3751
[24] Turkevich L A and Cohen M H 1984 *Ber. Bungenges. Phys. Chem.* **88** 292
[25] Tracy C A and McCoy B M 1975 *Phys. Rev.* B **12** 368
[26] Pandit R, Schick M and Wortis M 1982 *Phys. Rev.* B **26** 5112
[27] Nakanishi H and Fisher M E 1982 *Phys. Rev. Lett.* **49** 1565
[28] Tarazona P and Evans R 1983 *Mol. Phys.* **48** 799